Computational design of compounds for monolithic integration in optoelectronics

Tairan Wang* and N. Moll
Department of Physics, Massachusetts Institute of Technology, Cambridge, Massachusetts 02139

Kyeongjae Cho
Mechanics and Computation Division, Mechanical Engineering Department, Stanford University, Stanford, California 94305

J. D. Joannopoulos
Department of Physics, Massachusetts Institute of Technology, Cambridge, Massachusetts 02139
(Received 11 July 2000; published 27 December 2000)

A class of semiconductors is introduced and their physical properties are examined using both *ab initio* total-energy calculations and quasiparticle GW calculations. These compounds are designed to address problems of lattice-constant mismatch and polarity mismatch that are common issues in heteroepitaxial growth of III-V alloys on silicon substrates. A variety of configurations of these materials is explored. It is found that their lattice constants and band gaps fall into a region of phase space different from that of conventional semiconductors, making them potential candidates for the basis of optical devices—infrared emitters and detectors. A particular suitable configuration is identified that is lattice-constant matched to Si and has a direct band gap of 0.8 eV. This gap corresponds to the canonical wavelength of 1.5 μm in optoelectronics. Thus this material could ultimately enable tractable monolithic integration of optics with electronics. The characteristics of this particular configuration are examined in depth, including its temperature dependence, its bulk energetics, and its growth energetics. The results of these analyses indicate that fabrication of these compounds using heteroepitaxial growth techniques should be feasible.

DOI: 10.1103/PhysRevB.63.035306 PACS number(s): 71.15.Nc, 85.60.Bt

I. INTRODUCTION

In the optoelectronics industry, great efforts have been devoted to monolithically integrate electronic materials with optically active materials. As the sizes of electronic devices continue to shrink and the usage of optical communication continues to grow, monolithic integration becomes increasingly desirable and necessary. Various different approaches have been suggested, each with its own problems.[1–6]

One very natural approach is to heteroepitaxially grow optically active materials, such as GaAs for example, directly on top of Si.[3–6] However, there are two basic problems facing epitaxial growth of these optical materials on Si or Ge substrates. Firstly, heteropolar semiconductors, e.g., III-V's and II-VI's, are polar when grown along the (001) direction. This causes a polarity mismatch with the underlying group-IV substrate. Secondly, most existing optical materials and their alloys do not match lattice constant with Si or Ge. In Fig. 1, we plot the band gaps and the lattice constants for conventional semiconductor alloys that are currently used for optically active devices. The III-V alloys shown in Fig. 1 that exhibit band gaps matching the operating wavelength of optical fibers ($\sim$1.5 μm) have lattice constants about 8% larger than that of Si. Therefore, it is impossible to grow these alloys defect free on Si substrates. The polarity mismatch and the lattice mismatch make it exceedingly difficult to create optoelectronic integrated devices using heteroepitaxy.

As shown in Fig. 1, most of the existing materials have either larger lattice constants or larger band gaps than of interest. They lie in the upper right-hand section of the graph. The desired regions of the phase space, on the other hand, are the intersections of the gray regions. Our goal in this paper is to design materials that lie in the gray regions and have the following properties: Firstly, the materials should be polarity matched to the group-IV (001) surface. Secondly, the lattice constants of the materials should be between those of Si and Ge. This ensures that the materials would match lattice constants with suitable electronic substrates. Thirdly, as emitters are our primary interest, the materials should exhibit direct fundamental band gaps. Finally, their band gaps should correspond to one of the two currently interesting wavelength regions: the region around the canonical optical-fiber wavelength of 0.8 eV (1.5 μm), or the longer wavelength far-infrared region. By exhibiting all these properties, these materials could lead to infrared detectors and emitters that can be integrated monolithically with group-IV substrates.

It would be a formidable task, if not nearly impossible, to explore all these materials solely by growing and experimentally measuring their physical properties, since even the growth processes are still completely unknown. These processes would have to be established and refined first. Instead, we exploit the predictive and tractable power of *ab initio* calculations to obtain the properties of these materials, thus providing a screening for future experimental analysis of the most interesting examples of these materials.

This paper is organized as follows. We begin with a general description of the materials and how they solve the polarity mismatch in Sec. II. Next we describe the computational details in Sec. III. In Sec. IV we present an overview of the results for various configurations of these materials. Some potential applications for selected configurations are discussed in Sec. V. This includes a particularly interesting

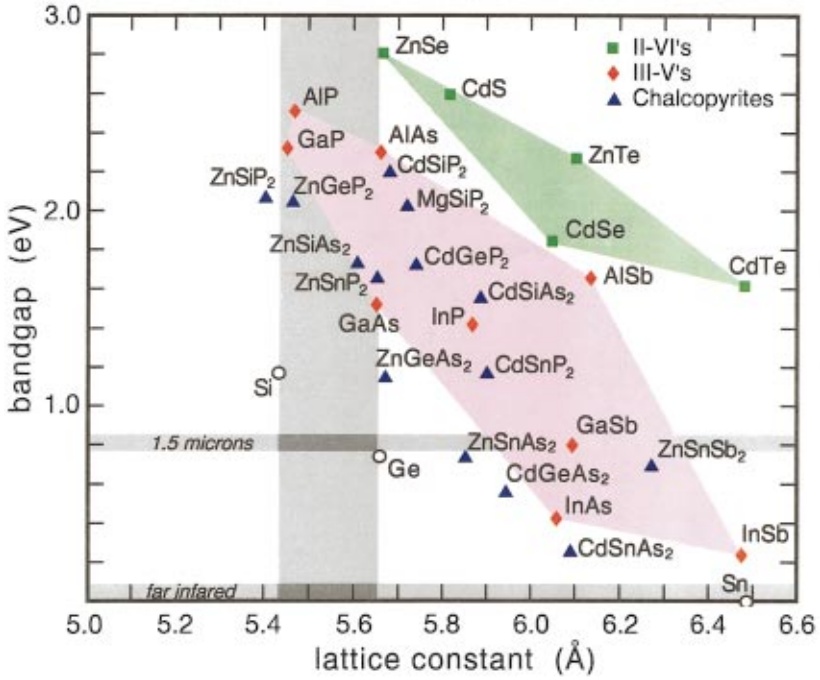

FIG. 1. (Color) Band gaps and lattice constants for various traditional semiconductor materials. The III-V's are shown in red diamonds, and the II-VI's are shown in green squares. The color-shaded areas denote possible alloyed materials. Also shown are the chalcopyrite materials in blue triangles. The gray regions correspond to lattice constant in between that of Si and Ge, and band gaps of the optical-fiber wavelength of 1.5 μm and the longer wavelength far-infrared regions.

configuration, $(ZnSi)_{1/2}P_{1/4}As_{3/4}$, that would be appropriate for monolithic integration with Si. Finally in Sec. VI, we explore the properties and characteristics of $(ZnSi)_{1/2}P_{1/4}As_{3/4}$ in depth. This includes its temperature dependence, its bulk energetics, and its growth energetics.

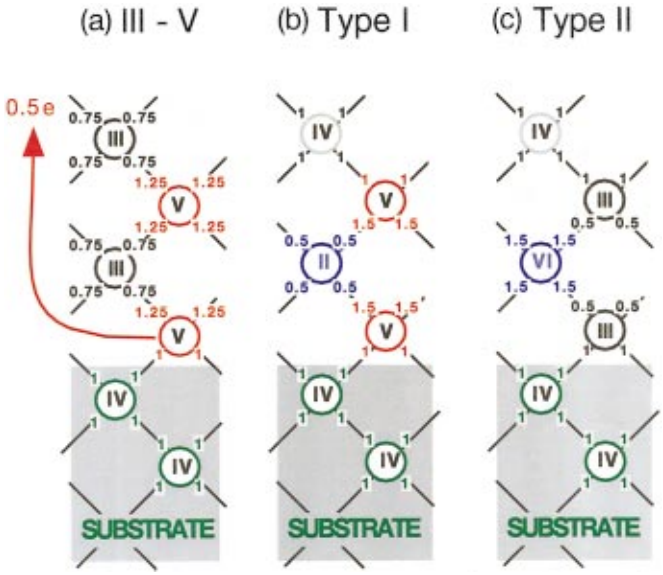

FIG. 2. (Color) Schematic illustration of bond saturation in (001) heteroepitaxial layering of Type I and Type II materials as compared with the layering of III–V's. The number of electrons contributed by each atom is indicated along each bond. Note that the atoms of Type I and Type II materials can satisfy their valency locally which resolves polarity-mismatch problem.

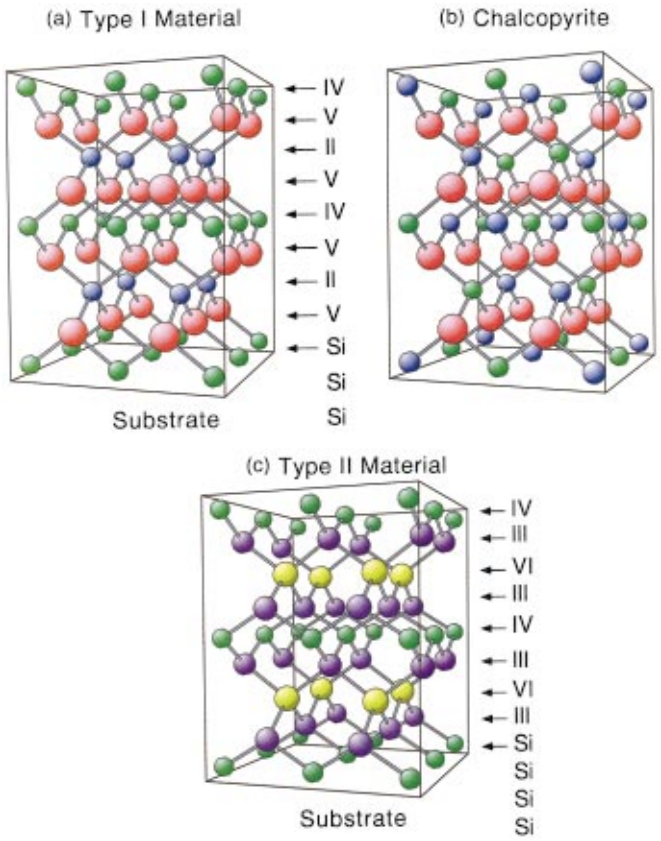

FIG. 3. (Color) Schematic atomic models of the crystal structures of Type I and Type II materials. For the Type I material, the corresponding chalcopyrite structure is also shown.

II. DESIGN OF A CLASS OF SEMICONDUCTORS

As the first requirement of the materials we address the polarity matching. The typical interface of a III-V compound on a group-IV (001) substrate is illustrated schematically in Fig. 2(a). Inside the bulk, a group-V atom possesses four bonds with its group-III neighbors, contributing 5/4 electrons to each bond. However, at the interface with the group-IV substrate, the group-V atom can only contribute one electron each to the two bonds with the substrate atoms in order to satisfy the two-electron-per-bond counting rule. Consequently, half an electron for every interface group-V atom is redistributed to the outer surface of the structure, creating a long-range electric field that is undesirable. This is the commonly known polarity-mismatch problem.[7]

Our solution to this problem is to reduce the valency of the second-layer atoms by one to accommodate the extra electrons from the interface group-V atoms, as is illustrated in Fig. 2(b).[8] In doing so, we also need to increase the valency of the fourth layer atoms by one. It is easy to see that all the bonds are now saturated locally, with no need for any long-range charge transfer. This layering process can then be repeated without generating a long-range field. We denote this class of materials as Type I materials. The charge-mismatch problem of the interface is now resolved.

Similarly, if we start with a group-III layer at the interface, then we can increase or decrease the valencies of the subsequent group-V layers [Fig. 2(c)]. We denote this class of materials as Type II materials.

These materials can be considered as *pseudo* III–V materials, with either the group-III element replaced by an equal mixture of group-II and group-IV elements, or the group-V element replaced by an equal mixture of group-IV and group-VI elements. The schematic atomic arrangement of the materials are illustrated in Fig. 3. Both the Type I and the Type II materials have layered atomic arrangement, which makes them amenable to epitaxial growth.

Note that the Type I materials have the same chemical formula as the naturally-occurring chalcopyrite materials.[9] The atomic structure of the chalcopyrites is shown in Fig. 3(b). Both the Type I and the chalcopyrite structures are distorted zinc-blende structures. However, the two atomic arrangements are rather different. In the chalcopyrites, the group-II and group-IV elements are intermixed to form effective group-III layers. Therefore, the chalcopyrites are polar materials when growing along the (001) direction. They exhibit the common polarity-mismatch problem while grown on an Si substrate. The atomic arrangement of the chalcopyrites also makes it more difficult to grow them by a layer-by-layer heteroepitaxial deposition. As naturally occurring materials, the chalcopyrites are the ground-state structures for bulk materials for the particular chemical formula.

For both the Type I and the Type II materials, there are many possible configurations that can be obtained by choosing different elements for the different groups. For example, one could create $(ZnSi)_{1/2}P$, where Zn is used for the group-II element, Si for the group-IV element, and P for the group-V element. In principle, any other elements of the different groups can be used. It is also possible to combine different Type I materials to create an alloy or, moreover, combine Type I and Type II materials together. Just as the traditional III-V, II-VI materials and their alloys, the Type-I and the Type-II materials span a wide range in terms of lattice parameters and band structures.

To explore this phase space, we begin with the simplest configurations, which consists of a chemical formula of only three elements. As a starting point, we used the tetrahedral-covalent radii of elements from Shay[9] to approximate the lattice constants of various configurations of the Type I and the Type II materials. The approximated lattice-constant mismatches to Si can be found in Ref. 8. These estimates are not too accurate, and have an error that we eventually find to be around 4% as compared to the *ab initio* calculations. Nevertheless, they served as a useful guide to identify the configurations that would most likely have lattice constants in the neighborhood of Si and Ge. To gain more accurate structural properties on these configurations, we employ *ab initio* total-energy calculations. Before we present the results of these calculations, we will describe the details of the computational methods in the next section.

III. COMPUTATIONAL DETAILS

To determine the structural properties, we carry out total-energy calculations using density functional theory.[10–13] We apply the local-density approximation (LDA) to the exchange-correlation functional, choosing the parameterization by Perdew and Zunger[14] of Ceperley and Alder's[15] data for the correlation energy of the homogeneous electron gas.

We employ *ab initio* norm-conserving pseudopotentials. The pseudopotentials for the first-row elements are created with the scheme of Rappe *et al.*[16] or of Troullier and Martins.[17] The other pseudopotentials are generated using Hamann's scheme.[18,19] For the group-II elements, we employ nonlinear core corrections to improve the transferability of these potentials. These corrections take the nonlinear exchange of core and valence electrons into account.[20] The semi-local pseudopotentials are further transformed into fully separable Kleinman-Bylander pseudopotentials,[21] with the *d* potential chosen as the local potential, with the exception of Ge, where *p* potential is chosen as the local potential.

The wave functions are expanded into plane waves[22] with a kinetic energy up to at least 20 Ry. For structures which include first-row elements we use 40 Ry. The electron density is calculated from special **k**-point sets,[23] their density in reciprocal space being equivalent to 384 **k**-points in the whole Brillouin zone of a four-atom cell. For surface calculations, a special **k**-point set with a density equivalent to 64 **k**-points in the whole 1×1 surface Brillouin zone is used. From calculations done with different cutoff energies and **k**-point densities, we found that the differences between the total energies of structures in our calculations are converged to within 10 meV with the chosen parameters. For structures with the same supercell, the energy differences are converged to within 5 meV.

The equilibrium lattice parameters for different configurations of the materials are found by minimizing the total energy. For each set of lattice parameters the ions are relaxed

TABLE I. Results of *ab initio* calculations for Type I materials. Fractional lattice-constant mismatch with Si is shown in the first column. Fractional deviation from ideal zinc-blende c/a ratio is shown in the second column. The third column shows the fundamental band gap calculated within the GW scheme for nonmetallic materials. In the last column, d, i, mi, sm, m refer to direct, indirect, marginally indirect (<0.1 eV), semi-metallic and metallic band gaps, respectively.

Material	$\Delta a/a_{\mathrm{Si}}$ (%)	$\Delta(c/a)$ (%)	$E_{\mathrm{Gap}}^{\mathrm{GW}}$ (eV)	Directness
$(BeSi)_{1/2}P$	−6.32	0.1	1.68	i
$(BeGe)_{1/2}P$	−4.75	−0.9	1.16	i
$(ZnSi)_{1/2}P$	−3.08	4.1	1.56	d
$(MgSi)_{1/2}P$	−2.82	11.7	1.93	mi
$(BeSi)_{1/2}As$	−2.30	−0.4	1.19	i
$(CdSi)_{1/2}P$	−0.94	13.0	1.22	mi
$(ZnGe)_{1/2}P$	−0.88	1.9	1.15	i
$(ZnC)_{1/2}Sb$	−0.84	11.8	–	m
$(BeGe)_{1/2}As$	−0.59	−1.5	0.53	i
$(MgGe)_{1/2}P$	−0.34	9.2	1.13	i
$(BeSn)_{1/2}P$	0.66	−1.6	0.98	i
$(ZnSi)_{1/2}As$	0.99	2.6	0.68	mi
$(MgSi)_{1/2}As$	1.34	10.2	0.93	mi
$(CdGe)_{1/2}P$	1.72	10.1	0.33	d
$(ZnGe)_{1/2}As$	3.09	0.7	0.23	mi
$(CdSi)_{1/2}As$	3.33	10.6	–	sm
$(MgGe)_{1/2}As$	3.95	7.3	–	sm
$(BeSn)_{1/2}As$	4.31	−2.1	0.45	i
$(ZnSn)_{1/2}P$	4.76	−0.8	1.70	i
$(CdGe)_{1/2}As$	5.99	7.9	–	m
$(ZnSn)_{1/2}As$	8.20	−1.3	0.79	mi

until the forces are smaller than 50 meV/Å. For the equilibrium structures we compute the band structures to investigate if they are optically active, and at what frequency range.

However, since LDA methods give inaccurate band gap results, we employ the GW approximation[24,25] for the electron self-energy to calculate the quasiparticle band structure to obtain accurate band-gap information. This method, which is fully based on first principles, has been shown to yield band structures in excellent agreement with experiment for a large class of materials including semiconductors.[26,27] Gap energies are usually given within an uncertainty in the order of 0.1 eV. We use the lattice parameters predicted by the LDA calculations for the GW calculations. With the obtained LDA wave functions and energy spectra, we determine the quasiparticle band structure using a procedure that has become state-of-the-art in band-structure calculations. We con-

TABLE II. Results of *ab initio* calculations for Type II materials. Fractional lattice-constant mismatch with Si is shown in the first column. Fractional deviation from ideal zinc-blende c/a ratio is shown in the second column. The third column shows the fundamental band gap for nonmetallic materials. In the last column, d, i, mi, sm, m refer to direct, indirect, marginally indirect (<0.1 eV), semi-metallic and metallic band gaps, respectively.

Material	$\Delta a/a_{\mathrm{Si}}$ (%)	$\Delta(c/a)$ (%)	$E_{\mathrm{Gap}}^{\mathrm{GW}}$ (eV)	Directness
$Al(CTe)_{1/2}$	−5.54	10.1	–	m
$Ga(CTe)_{1/2}$	−4.91	9.5	–	m
$B(SnTe)_{1/2}$	−2.49	0.3	0.66	d
$In(CS)_{1/2}$	2.30	4.2	0.88	d
$In(CSe)_{1/2}$	3.43	6.6	0.02	d
$Ga(SiS)_{1/2}$	3.87	−5.9	1.16	mi
$Ga(GeS)_{1/2}$	4.75	−6.1	0.91	d
$Al(SiS)_{1/2}$	4.94	−6.9	1.25	d
$Ga(SiSe)_{1/2}$	5.29	−3.4	1.27	i
$Al(GeS)_{1/2}$	5.69	−7.6	1.04	d
$Al(SiSe)_{1/2}$	6.55	−3.8	1.39	i

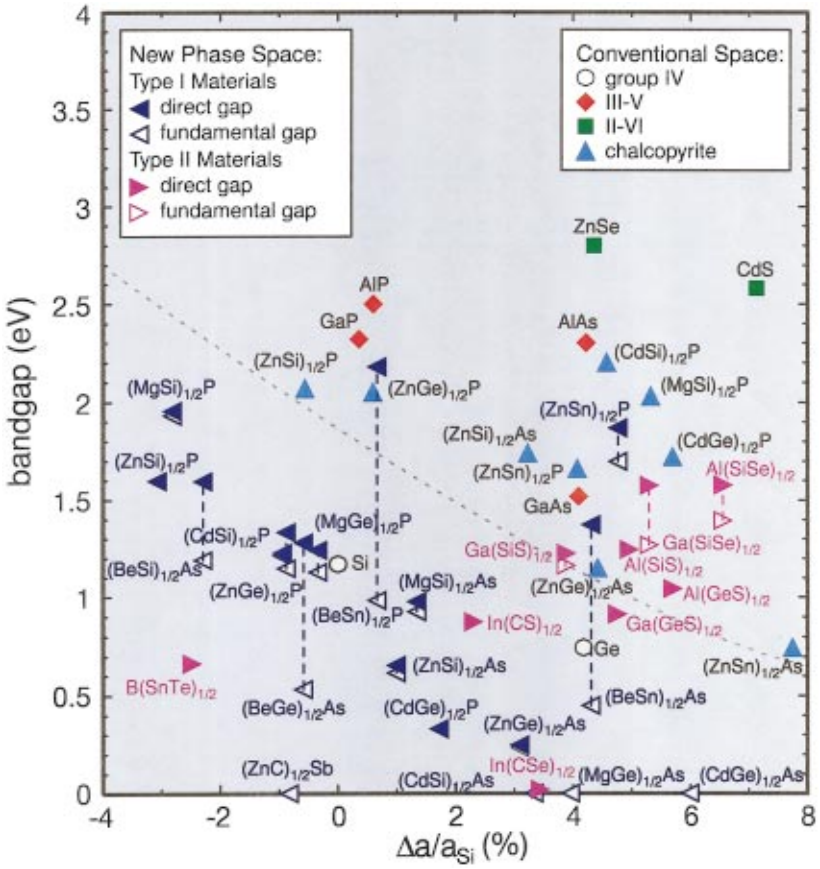

FIG. 4. (Color) The lattice constants as calculated within the LDA approximation, and the band gaps as calculated within the GW approximation. The light blue left-triangles are Type I materials, and the red right-triangles are Type II materials. The filled symbols indicate the sizes of direct gaps, while the open symbols indicate the sizes of fundamental gaps for the indirect band-gap materials. For metallic materials, only open symbols are shown. For reference, we also include the experimental values of the traditional semiconductors. III-V materials are shown in red diamonds; II-VI materials are shown in green squares; and some of the chalcopyrite materials are shown in blue triangles. The gray dashed line indicates the lower boundary of the phase space spanned by the conventional optical materials.

struct the electron self-energy operator within the GW approximation. The difference between the GW self-energy operator and the LDA exchange-correlation potential constitutes the quasiparticle corrections to the LDA band structure, thus leading to the quasiparticle band structure. To obtain good band-gap information for materials involving As, the *s* potential is chosen as the local potential for the band-gap calculations.

IV. OVERVIEW OF RESULTS

The *ab initio* lattice constants and the GW band gaps calculated for the Type I materials are summarized in Table I. The lattice constants of the Type I materials span a wide range, covering the Si lattice constant. They tend to have smaller lattice constants and smaller band gaps than their chalcopyrite counterparts. There are a couple of configurations with direct band gaps, and quite a few with marginally indirect gaps. However, neither direct band-gap materials matches lattice constant with Si. $(ZnSi)_{1/2}P$ is 3% too small, and $(CdGe)_{1/2}P$ is 2% too large. The c/a ratios also show a wide range of values, covering the ratio of the ideal zinc-blende structure. In general, group-IV and group-V elements with larger covalent radii lead to smaller c/a ratios, while group-II elements with larger covalent radii lead to larger c/a ratios.

The results of *ab initio* calculations of the Type II materials are summarized in Table II. The lattice constants of the Type II materials are either too small or too large compared to that of Si. There is no configuration within 2% of Si, although there are several around the lattice constant of Ge. There are, however, half a dozen direct band-gap Type II configurations. The direct band-gap materials are the focus of the next section. The c/a ratios again cover a wide range. In general, group-VI elements with larger covalent radii lead to larger c/a ratios, while group-IV elements with larger covalent radii lead to smaller c/a ratios.

Our results of the Type I and Type II materials are summarized in the lattice constant versus band-gap plot in Fig. 4, together with the traditional semiconductors. Although the materials are composed of elements found in the traditional semiconductors, they are quite far away in this phase space from the traditional semiconductors.

We also applied the same computational methods to the traditional semiconductors to gauge our accuracy. For this purpose, we calculated the lattice parameters of the group-IV

TABLE III. Direct band-gap materials. The second column lists the percentage lattice-constant differences compared with that of Si. The last two columns list the GW band gaps in eV and μm.

Material	$\Delta a/a_{\mathrm{Si}}$ (%)	$E_{\mathrm{Gap}}^{\mathrm{GW}}$ (eV)	$E_{\mathrm{Gap}}^{\mathrm{GW}}$ (μm)
$(ZnSi)_{1/2}P$	−3.08	1.56	0.8
$B(SnTe)_{1/2}$	−2.49	0.66	1.9
$(CdGe)_{1/2}P$	1.72	0.33	3.8
$In(CS)_{1/2}$	2.30	0.88	1.4
$In(CSe)_{1/2}$	3.43	0.02	60
$Ga(GeS)_{1/2}$	4.75	0.91	1.4
$Al(SiS)_{1/2}$	4.94	1.25	1.0
$Al(GeS)_{1/2}$	5.69	1.04	1.2

elements in the diamond structure, the III-V and the II-VI materials in zinc-blende structure, and finally the chalcopyrite materials. The lattice constants obtained are in fairly close agreement with experimental values. Most are within 2%. A notable exception is CdS, which has a calculated lattice constant 4% larger than the experimental value. We attribute this effect to the larger size difference between Cd and S ions, which heightens the error introduced by the frozen-core approximation. In comparison, the lattice parameters of the chalcopyrite materials which contain either Cd or S have fairly good agreement with experimental values. The GW band gaps obtained for the traditional semiconductors also agree very well with previously published results which have an error of 0.1 eV in band gap as compared to experimental results.

V. SOME PROMISING CONFIGURATIONS FOR APPLICATIONS

With the properties of many Type I and Type II materials in hand, we proceed to discuss their potential applications in this section. We first look at the direct band-gap materials as potential light emitter and detector materials. We then examine the indirect band-gap materials as possible useful detectors.

A. Emitters

If the fundamental band gap of a material is direct, as is the case for GaAs, the material can potentially be both a good light emitter and detector. Therefore, it can be employed as the basis for semiconductor diodes or lasers. There are several Type I and Type II materials which possess direct band gaps. They are summarized in Table III.

Three of the configurations, $Ga(GeS)_{1/2}$, $Al(SiS)_{1/2}$, and $Al(GeS)_{1/2}$, have lattice constants larger than that of Ge. Their band gaps are around 1 eV, and a bit larger than the canonical optical fiber frequency of 0.78 eV. One option for growing these materials on top of a Ge substrate is to alternatively grow thin layers of these materials and layers of Ge. This could contain the strain caused by the lattice mismatch.

The next three configurations, $(CdGe)_{1/2}P$, $In(CS)_{1/2}$, and $In(CSe)_{1/2}$, have lattice constants somewhere in between that of Si and Ge. It should be possible to grow these on top of Si-Ge alloys. $In(CS)_{1/2}$ has a gap very close to the optical fiber frequency. $In(CSe)_{1/2}$ has a very small gap, making it a potential candidate for a far-infrared emitter. If one alloys these two materials, one can potentially tune the band gap anywhere in between.

Finally, $B(SnTe)_{1/2}$ and $(ZnSi)_{1/2}P$ have lattice constants quite smaller than that of Si. Possible substrates for these two materials are Si-C alloys. Furthermore, $(ZnSi)_{1/2}P$ is interesting in other respects which is described in the following.

We consider now the option of alloying two Type I materials to design a material for monolithic integration with Si. Two possible candidates are $(ZnSi)_{1/2}P$ which has a direct band gap and $(ZnSi)_{1/2}As$ which has an indirect band gap as shown in Table I and Fig. 4. We create an ordered alloy with both materials to obtain a material that is lattice matched to Si and has a direct band gap at the canonical optical-fiber frequency. The material $(ZnSi)_{1/2}P$ has a lattice constant that is too small and a direct band gap that is too large. On the other hand, the material $(ZnSi)_{1/2}As$ has a lattice constant which is too large and a band gap which is too small and marginally indirect. We denote the ordered alloy of these two materials as $(ZnSi)_{1/2}P_xAs_{1-x}$ where x is the P concentration. The *ab initio* results for the calculated GW band gap and lattice mismatch are shown in Fig. 5 as a function of the P concentration. With increasing P concentration the lattice constant decreases and the band gap increases and becomes direct. At a P concentration of 1/4, the lattice constant almost matches that of Si perfectly. Moreover, the band gap almost matches the canonical optical-fiber frequency and is direct. This optimal material has the chemical formula $(ZnSi)_{1/2}P_{1/4}As_{3/4}$. Its atomic structure is the $(ZnSi)_{1/2}As$ structure where every fourth As layer is substituted by a P layer. This ordered alloy is a good candidate for a light-emitting material grown on Si. Note, this optimal material possesses a slight dipole moment due to the difference in chemical properties of P and As. However, this dipole moment can be eliminated if we invert every other cell in the growth direction, i.e., use a supercell twice as long in the growth direction.

It is fortunate that we have achieved both lattice matching and band-gap matching with a single parameter. To compensate for errors in the predicted lattice constants and band gaps, one can tune the physical parameters by changing the P concentration, by changing the specific layering order of the layers of P and As, and by changing some other layers, e.g.,

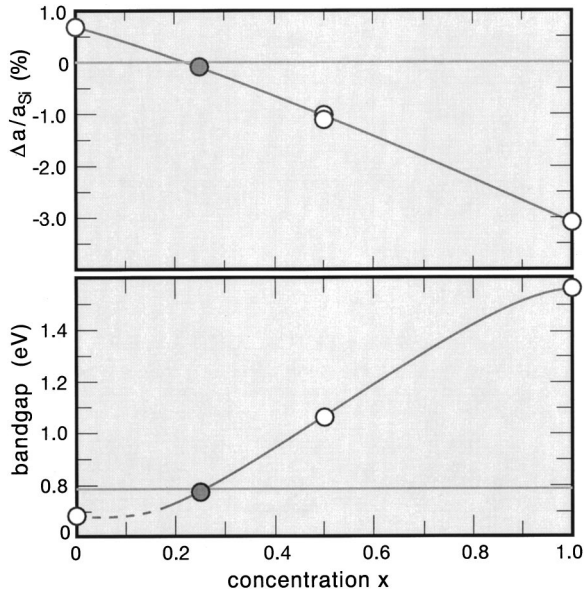

FIG. 5. The lattice-constant mismatch (top panel) and GW band gap (bottom panel) for $(ZnSi)_{1/2}P_xAs_{1-x}$ as a function of the P concentration x. The dashed line in the bottom panel represents the region where the band gap is indirect.

use Ge in place of Si in some layers. Thus, the precision of the lattice matching and the band-gap matching is not as important as the possibility of tuning these parameters.

From the LDA band structure, we calculate the carrier effective masses for this optimal material. The electron effective mass at the conduction-band minimum is about 0.5 m_e in the (001) direction, 0.3 m_e, and 1.2 m_e perpendicular to that. For the holes, the effective mass is 0.7 m_e along (001) direction, and 25 m_e and 0.6 m_e in the other two principal-axis directions.

B. Detectors

Even if a material does not have a direct fundamental gap, it could still be used as a light detector. The minimum direct band gap gives a good indication of the range of frequency in which the material may be suitable as a detector.

In Table IV, we summarize several materials that are closely matched in lattice constant to either Si or Ge. The first three materials—$(BeSn)_{1/2}P$, $(CdSi)_{1/2}P$, and $(MgGe)_{1/2}P$ have lattice constants close to Si and could possibly be grown directly on a Si substrate. While the other three materials—$(BeSn)_{1/2}As$, $(ZnSn)_{1/2}P$, and $Ga(SiS)_{1/2}$ have lattice constants close to Ge and could possibly be grown on top of Ge.

The materials $(CdSi)_{1/2}P$, $(MgGe)_{1/2}P$, $Ga(SiS)_{1/2}$ have a band gap of 1.2 eV. The material $(BeSn)_{1/2}As$ has a band gap of 1.4 eV. The materials $(BeSn)_{1/2}P$ and $(ZnSn)_{1/2}P$ have a band gap around 2 eV. In comparison, the direct band gap of Si is more than 3 eV. The band gaps of these materials are within the range of what would be appropriate for solar cell applications.[28]

VI. CHARACTERISTICS OF $(ZnSi)_{1/2}P_{1/4}As_{3/4}$

In the previous section, we have examined and discussed the general properties of the bulk Type I and Type II materials. We now focus on the configuration $(ZnSi)_{1/2}P_{1/4}As_{3/4}$ which is lattice matched to Si and has a direct band gap of 0.8 eV. We analyze in depth its characteristics, including its temperature dependence, bulk energetics, and growth energetics. In some of the calculations we use $(ZnSi)_{1/2}As$ as a prototype instead of the optimal material $(ZnSi)_{1/2}P_{1/4}As_{3/4}$ for simplicity and to reduce the computational complexity. However, all the conclusions derived for $(ZnSi)_{1/2}As$ also apply to the optimal configuration $(ZnSi)_{1/2}P_{1/4}As_{3/4}$.

A. Temperature dependence

So far, we have only examined the properties of the materials at zero temperature. Temperature effects on the lattice constant could potentially alter the level of lattice matching from that at zero temperature. To judge the importance of this effect, we estimate the thermal-expansion coefficients from the total-energy surfaces for $(ZnSi)_{1/2}P_{1/4}As_{3/4}$ and Si. For this we use the anharmonicities of the elastic energies. The expectation value of the lattice constant for a finite temperature is given by

$$\langle a\rangle_T = \frac{1}{Z}\int a \exp^{-E_{tot}(a)/kT} da, \tag{1}$$

where Z is the partition function. From this expectation value we calculate the relative lattice expansion for both materials, as shown in Fig. 6. The difference of the relative lattice expansion is less than 0.01% from 0 to 600 K. This suggests that, for this particular Type I material, thermal expansion will not alter significantly the level of lattice matching from the zero-temperature results. The band gaps will also be in-

TABLE IV. Potential detector materials. The lattice constants are in the neighborhood of Si or Ge. The GW band gaps, in eV and μm, are listed in the last two columns.

Material	a	$E_{\mathrm{Gap}}^{\mathrm{GW}}$ (eV)	$E_{\mathrm{Gap}}^{\mathrm{GW}}$ (μm)
$(BeSn)_{1/2}P$	1% Si	2.2	0.6
$(CdSi)_{1/2}P$	1% Si	1.2	1.0
$(MgGe)_{1/2}P$	1% Si	1.2	1.0
$(BeSn)_{1/2}As$	1% Ge	1.4	0.9
$(ZnSn)_{1/2}P$	1% Ge	1.9	0.7
$Ga(SiS)_{1/2}$	1% Ge	1.2	1.0

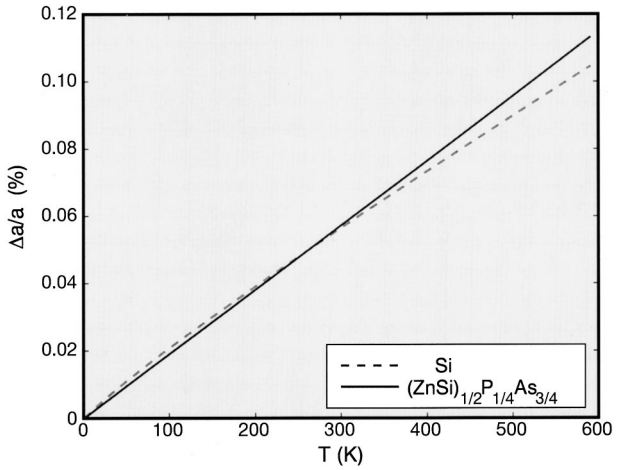

FIG. 6. Relative lattice expansion $(a(T)-a(0))/a(0)$ for Si and $(ZnSi)_{1/2}P_{1/4}As_{3/4}$ as a function of the temperature T. There is no significant additional lattice mismatch at higher temperatures.

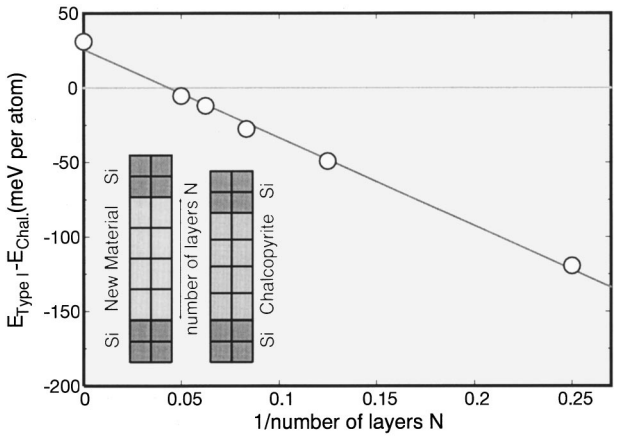

FIG. 7. Total-energy difference $E_{\text{Type I}}-E_{\text{Chal}}$ between the Type I material $(ZnSi)_{1/2}As$ and its chalcopyrite counterpart in a heterostructure arrangement. N is the number of atomic layers in the (001) direction.

fluenced by temperature. Traditional III-V semiconductors (both direct and indirect band-gap materials) typically exhibit 3%–6% drop in their band gaps going from zero temperature to room temperature.[29] We expect these materials to be influenced similarly. This can be countered by changing the P concentration, by changing the specific layering orders of the layers of P and As, or by changing the elements in some other layers. For example, to increase the band gap by 5% one needs only to increase the P concentration to 33%. This would lead to a still very small lattice mismatch of only -0.3%.

B. Bulk energetics

As mentioned earlier, Type I materials actually share the same chemical formula as the chalcopyrite materials, with the latter being the ground-state configuration. In this section we compare the bulk energetics of both materials. For simplicity in comparing with the chalcopyrite structure, we use $(ZnSi)_{1/2}As$ instead of the optimal material $(ZnSi)_{1/2}P_{1/4}As_{3/4}$. However, the general conclusions apply to the optimal material as well, which is discussed at the end of this section.

The calculated formation enthalpy of the chalcopyrite structure of $(ZnSi)_{1/2}As$ is 148 meV per atom. In comparison, the Type I structure of $(ZnSi)_{1/2}As$ has a formation enthalpy of only 83 meV per atom. Thus, the Type I material is chemically stable against segregation, just as the chalcopyrite is, but the Type I material is only metastable compared with the chalcopyrite form. However, to convert the Type-I material to the chalcopyrite form, two second neighbors have to be exchanged. We expect the diffusion barrier to be quite high because interstitials have to be created. Therefore, the diffusion process is very unlikely to occur under normal conditions after fabrication. In fact, as shown later, single chalcopyritelike defects are energetically unfavorable and a substantial region of defects has to be created to gain energy. This will additionally stabilize our material once it is fabricated.

As a next step we examine the potential growth of these two types of material structures on a Si substrate. The Type-I structure is favored in two respects. We note that both the lattice constants and polarities are different for the two structures. We begin by examining the effects of lattice-constant matching. The formation energies of both structures are computed for geometries where they are constrained horizontally to the Si lattice constant. This corresponds to the initial growth of both structures on Si. The bulk energy difference between the two counterparts is reduced from the free bulk case of 65 meV per atom to 31 meV per atom. The energy difference becomes smaller because the Type I $(ZnSi)_{1/2}As$ structure has a closer lattice-constant match with Si than the chalcopyrite form and thus a smaller strain energy when grown on Si. Nevertheless, the bulk chalcopyrite structure is still lower in energy.

To obtain quantitative results on how the polarity matching of the Type-I material affects the energetics, we compare two heterostructures where either the Type I structure, or the chalcopyrite structure, is sandwiched between Si. This geometry and the difference of the total energies as a function of the reciprocal of the number of layers is shown in Fig. 7. The calculations are performed in the following way. The supercell consists of four layers of Si, and N atomic layers in the (001) direction of either of the two $(ZnSi)_{1/2}As$ structures. The calculations are performed for N equal to 4, 8, 12, 16, and 20. The lattice constant in the horizontal direction is kept fixed at the Si lattice constant. The supercell is allowed to relax in the (001) direction. The atoms are also allowed to relax within the cell.

The difference of the total energies is linear in the reciprocal of the number of layers. This can be easily understood. The total-energy difference has two contributions. The first contribution is the bulk energy difference between the two configurations. The second contribution is the interface energy difference between the two configurations. The chalcopyrite structure has a different interface with the Si substrate than the Type I structure. Therefore, the energy difference per atom has to take the following form

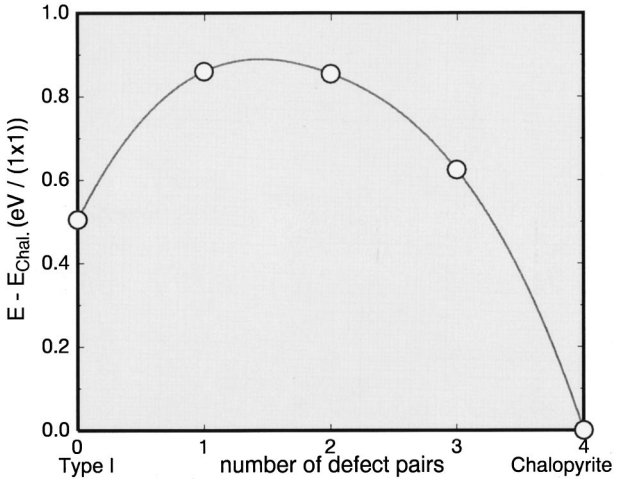

FIG. 8. Total energies of $(ZnSi)_{1/2}As$ with various number of defects. Each defect corresponds to the mixing of a pair of neighboring Si/Zn layers. The structure with four defects becomes the chalcopyrite structure in this supercell with 16 layers in the (100) direction. The chalcopyrite structure is chosen as the reference structure.

$$E_{\text{Type I}} - E_{\text{Chal}} = \Delta E_0 + \frac{\Delta \gamma_{\text{int}}}{N}, \tag{2}$$

where ΔE_0 is the bulk energy difference, $\Delta \gamma_{\text{int}}$ captures the difference in interface energies, and N is the number of atomic layers of $(ZnSi)_{1/2}As$ in the (001) direction. The interface energy difference $\Delta \gamma_{\text{int}}$ is negative, reflecting the higher interface energy between the chalcopyrite form and the Si substrate. The Type I structure is actually the more stable form for N smaller than 22 atomic layers. Therefore, if one deposits three extra atomic layers of Si for about every 20 atomic layers of Type I structure, then it should be possible to significantly extend the thickness of the region of Type I structure.

As a next step we examine the energetics for creating chalcopyritelike defects in the Type-I structure. The Type I $(ZnSi)_{1/2}As$ bulk is represented by a supercell of 16 atomic layers in the (001) direction, and with a cross section of $c(2\times 2)$ which is constrained to Si bulk lattice constant. We then proceed to create various numbers defect pairs by mixing neighboring layers of Si and Zn atoms. The energy difference of these various structures are shown in Fig. 8 with the chalcopyrite structure being the reference structure. Mixing two neighboring Si and Zn layers costs 0.36 eV in energy compared to the energy of the material structure. This value is consistent with 0.40 eV which we find to be the energy cost of creating a pair of defects by exchanging two neighboring Si and Zn atoms in a 64-atom Type I supercell. An approximately contiguous region of at least 4 Si/Zn layer pairs, corresponding to 16 atomic layers, have to be mixed to gain energy. Thus, a substantial region of the Type I structure has to be converted to the chalcopyrite form before the defect structure becomes energetically favorable. This further strengthens our belief that the Type I structure, once fabricated, will be stable instead of reverting to the chalcopyrite form.

Finally, we expect all of the above trends to be applicable to the optimal-layered Type I structure of $(ZnSi)_{1/2}P_{1/4}As_{3/4}$. This Type I material has a bulk energy 45 meV per atom higher than the corresponding chalcopyrite structure. When constrained to the Si lattice constant horizontally, this difference is reduced only by 5 meV per atom to 40 meV per atom. The chalcopyrite structure is still favored. When creating a multiwell structure of eight atomic layers of the Type I structure sandwiched between Si substrates, the Type I structure is energetically favored by 41 meV per atom. We expect that the difference of the total energy should again be linear versus the reciprocal of the number of layers. Thus the energy difference should cross zero at around 16 atomic layers, corresponding to two unit cells in the (001) direction. Thus, if three extra atomic layers of Si are deposited for every two unit cells of the Type I structure grown, the resulting structure should be stable compared with the chalcopyrite form.

In the above discussion, we have not examined all the possible arrangements of P and As atoms in the group-V sites. For example, P and As can be mixed in the same layer, without sacrificing too much of the polarity matching with the Si substrate. Since polarity matching is the critical difference between Type I structure and its chalcopyrite counterpart, we expect the structures with different P/As arrangement to have similar energies, but are currently beyond the scope of this study.

C. Growth

Another important question regarding the materials is whether they can be grown successfully using the prescribed layer-by-layer method. In this section, we are interested in the initial growth stages of the $(ZnSi)_{1/2}P_{1/4}As_{3/4}$ ordered alloy. For simplicity in comparing to the chalcopyrite structure, we again use $(ZnSi)_{1/2}As$ as a prototype.

First, we analyze qualitatively the layer-by-layer growth from the perspective of chemical bonding of layers with the substrates and apply the electron-counting rule. In Fig. 9 the different growth stages are shown schematically.

The first layer of As atoms deposited on top of a Si substrate would appear as shown in Fig. 9(a). The formation of such a layer is well known in the growth of III-V materials on Si substrates.[30] This initial deposition should therefore not pose too much difficulty. Note that the dimer reconstruction on the surface is not buckled. This can be understood as follows. There are three electrons per atom left in the dangling bonds of the As atom. When dimers are formed, every surface atom has two electrons left, saturating the dangling bond for each atom.

The next step is to deposit a layer of Zn atoms as shown in Fig. 9(b). From electron counting it follows that the As-terminated surface is equivalent to a group-VI terminated II-VI surface. The dangling bonds of the surface atoms are completely filled. Thus, growing the Zn layer should be analogous to the epitaxial growth process of a II-VI material. This process has been demonstrated experimentally to be possible.[31] There is one electron per atom left in the dangling

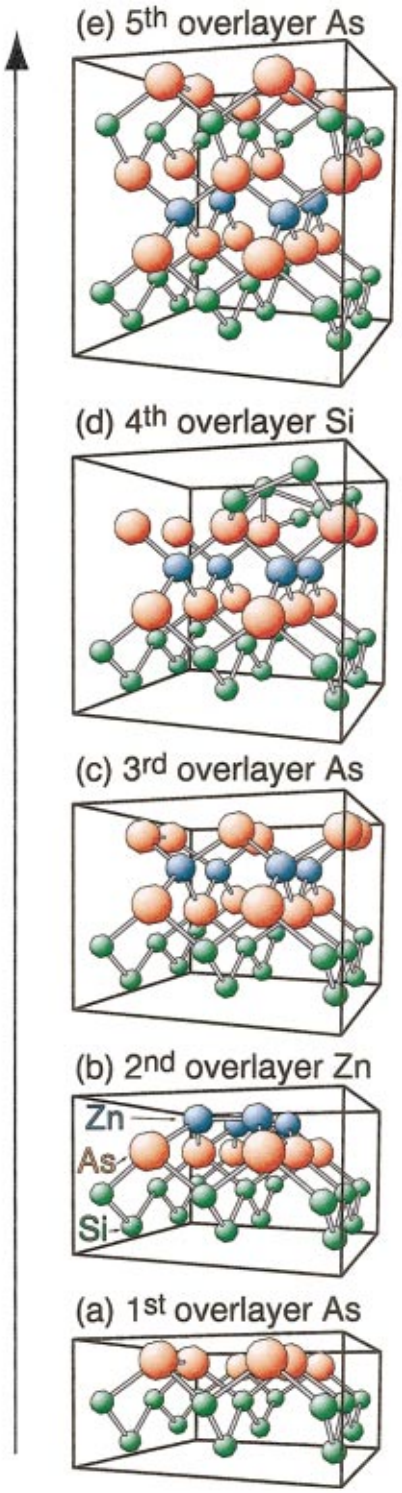

FIG. 9. (Color) Schematic illustration of the growth of Type I $(ZnSi)_{1/2}As$ on top of Si substrate.

bonds of Zn surface atoms. This is just enough to form a dimer bond, leaving the dangling bonds empty. The dimer is again unbuckled.

In the next step a layer of As atoms is deposited. For the As atoms the Zn terminated surface is equivalent to a II-terminated II-VI substrate [Fig. 9(c)]. This process has also been demonstrated in the laboratory.[32] The dangling bonds of each As surface atom contain two electrons. In analogy with the Si (100) surface, buckled dimers are formed and one electron is transferred across the dimer. The dangling bond of one dimer atom is filled, and the dangling bond of the other dimer atom is empty.

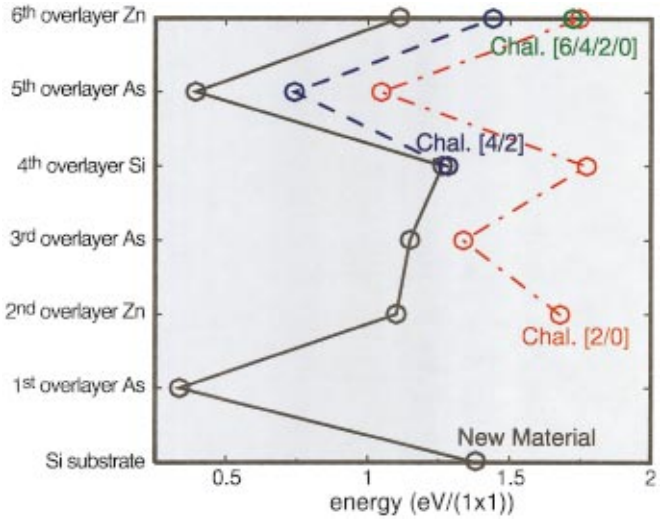

FIG. 10. (Color) Surface energies of the Type I $(ZnSi)_{1/2}As$ structure and various chalcopyritelike variants growing on Si(001). The Type I structures are shown in the black solid line; the cases where the second overlayer Zn atoms and the top layer atoms of Si substrate are intermixed are shown by the red dash-dot line; the cases where the fourth overlayer Si and the second layer Zn atoms are intermixed are shown by the blue dash line; and the maximum possible intermix involving all the Si and Zn layers when six overlayers are grown is shown in green. For some examples of different Type I overlayer structures, see Fig. 9.

Finally, when the next layer of Si atoms is deposited, the Si atoms encounter a surface with precisely one electron in each dangling bond, i.e., the same as a bare Si substrate [Fig. 9(d)]. Then the process repeats itself. In all cases, surfaces can be reconstructed into dimers. They are not metallic and should exhibit a low-surface energy.

To place these arguments on a more quantitative basis, we perform *ab initio* total-energy calculations for the different surfaces which occur during potential growth of Type I structures. The Si substrate is represented by four Si layers. The bottom layer is fixed, and electronically terminated on the bottom side with hydrogens. The growth then proceeds in the (001) direction, with a segment of vacuum equivalent to six atomic layers on the top to isolate the system from its image in the next supercell. The surfaces are allowed to reconstruct into dimers. The dimers are either flat or buckled, depending on the number of electrons in the dangling bonds as described above. Depending on whether the dimers are buckled or unbuckled we choose $c(2\times2)$, (2×1), and (4×2) as the surface cells. At every growth stage we calculate the surface energies of the Type I surface and the possible chalcopyritelike variants. These variants involve intermixing Si and Zn layers. Then, we can explore whether the Type I structures are stable or whether one of the chalcopyritelike variants are lower in energy.

The surface free energy for a particular structure is given by

$$\gamma_{\text{surface}}A = E_{\text{tot}} - \mu_{\text{Zn}}N_{\text{Zn}} - \mu_{\text{Si}}N_{\text{Si}} - \mu_{\text{As}}N_{\text{As}}. \quad (3)$$

E_{tot} is the total energy of the structure from the total-energy calculation. The chemical potential μ_i is the free energy per particle in the reservoir for the species i, and N_i denotes the number of particles of the species i in the structure.

The upper limit of each chemical potential is determined by the condensed phase of the respective elements,

$$\mu_i < \mu_{i(\text{bulk})}. \quad (4)$$

Otherwise, the elemental phase would form on the surface. Furthermore, in thermodynamic equilibrium, we have two additional equations, concerning the Si bulk and the Type I $(\text{ZnSi})_{1/2}\text{As}$ bulk,

$$\mu_{\text{Si}} = \mu_{\text{Si(bulk)}} \quad (5)$$

$$\mu_{(\text{ZnSi})_{1/2}\text{As}} = \mu_{\text{Zn}} + \mu_{\text{Si}} + 2\mu_{\text{As}} = \mu_{\text{Zn(bulk)}} + \mu_{\text{Si(bulk)}} + 2\mu_{\text{As(bulk)}} - \Delta H_f. \quad (6)$$

In this case ΔH_f is the heat of formation of the Type I structure while constrained to the Si lattice constant. We include the strain in the bulk energy so that the remaining energy is only due to the surface. This leaves us with one free parameter, which we choose to be μ_{As}. Using Eqs. (4), (5), and (6), μ_{As} can vary within the following range

$$\mu_{\text{As(bulk)}} - \frac{\Delta H_f}{2} < \mu_{\text{As}} < \mu_{\text{As(bulk)}}. \quad (7)$$

In Fig. 10, the surface energies of the different growth stages of $(\text{ZnSi})_{1/2}\text{As}$ are plotted (solid lines), together with those of the corresponding chalcopyritelike variants (dashed lines). Since there is usually an As over-pressure during typical growth conditions, we choose the As chemical potential to be the bulk value for this plot. For the corresponding chalcopyritelike variants, we use the same chemical potential for the bulk of $(\text{ZnSi})_{1/2}\text{As}$ so that in Fig. 10 the energy differences between structures at the same growth stage are the same as the total-energy differences. The energy of the chalcopyrite structures includes both the surface energy and the bulk energy difference between the chalcopyritelike structures and the Type I structure. Note that the comparisons between Type I structures and their corresponding chalcopyrite variants with the same number of growth layers are independent of the particular chemical potentials used, since they involve the same number of atoms for each species.

From Fig. 10, we see that during this initial growth stage, surfaces of the Type I structure are consistently lower in energy than various chalcopyrite variants. The closest competition comes at the fourth overlayer Si surface, where the Type I structure is only 0.03 eV lower in energy than the chalcopyrite variant. For the Type I structures, (2×1) supercells are the lowest-energy configurations for surfaces with flat dimers, while (4×2) supercells are the lowest-energy configurations for surfaces with buckled dimers. The chalcopyrite variants can not take advantage of the larger surface cells and the energy differences between the (4×2) and the $c(2\times2)$ cell are much smaller.

The different relative energies at different growth stages can be attributed to the energies of the different interfaces and surfaces. For example, when the growth reaches the second overlayer Zn surface, a competing chalcopyrite form mixes the surface Zn and the top layer Si atoms of the substrate, thus introducing an interface of Si with Si/Zn. The electron countings are identical for both surfaces and both surfaces form flat dimers. Thus, we expect the two surface energies to be similar. The Si–Si/Zn interface energy is calculated separately to be about 0.6 eV/(1×1) for As poor and 0.7 eV/(1×1) for As rich environments. This accounts for almost the entire difference between the two structures. Our expectation that the surface energies are similar in this case is thus confirmed.

Using the same argument we can explain why for the case of the fourth overlayer Si surface, the chalcopyritelike structure is so low in energy. For the chalcopyritelike structure the surface Si atoms are mixed with the second overlayer Zn atoms. This creates a Si–As interface instead of the Si–Si/Zn interface like in the previous case. The difference between the surfaces is again expected to be small. However, the energy of Si–As interface is calculated to be only 0.1 eV/(1×1) for As poor and 0.0 eV/(1×1) for As rich environments. This roughly explains why the chalcopyritelike structure has a low energy in this case.

The fact that the Type I surfaces are lower in energy is very encouraging. It implies that the growth elements will tend to nucleate in the Type I configuration. Once the Type I structure is formed, converting into the chalcopyrite structure involves second-neighbor exchange and a large energy barrier after fabrication. Furthermore, even if defects do form on certain surfaces, the energy cost associated with them will increase as more layers are added onto the top. This is supported by the fact stated earlier that single chalcopyritelike defects are not energetically favorable inside Type I bulk. All these points suggest that growth of the Type I structure on top of Si substrate should indeed be possible.

So far, we have only considered the dimer surface reconstructions. The dimer surface is the most common reconstruction and as our calculations show, these surfaces have low-surface energies that are comparable to that of Si (100). Under actual growth conditions, more complicated reconstructions could occur. The subsequent growth could then follow very different pathways. Nevertheless, this simple analysis provides us with a reasonable first step towards understanding this very complex system.

At last, we also note that one can discuss the growth of Type II materials in a similar fashion. The first layer involves the growth of a group-III layer on top of a group-IV substrate. The second layer of a group-VI layer is grown on top of a substrate analogous to a group-II-terminated II-VI substrate. The next group-III layer is grown on top of a substrate analogous to a group-VI-terminated II-VI substrate. Finally, the group-IV layer is grown on top of a group-IV like substrate.

VII. SUMMARY AND CONCLUSION

We have introduced a class of compound semiconductors that should be amenable to layer-by-layer epitaxial growth. The different possible combinations of elements provide a wide range of lattice constants and band gaps. We have employed *ab initio* total-energy calculations and quasiparticle GW computations to explore the properties of these compounds. Several interesting configurations for infrared emitters have been identified.

A particular configuration $(ZnSi)_{1/2}P_{1/4}As_{3/4}$ is lattice-constant matched to Si and has a direct band gap of 0.8 eV. It could lead to monolithic integration of optical materials and Si circuits. Estimated thermal expansion coefficients indicate that the lattice constant continues to match at room temperature.

Other configurations with potentially interesting applications are $In(CS)_{1/2}$ and $In(CSe)_{1/2}$. $In(CS)_{1/2}$ has a direct band gap of 0.88 eV in the range of the optical fiber frequency and could be used on Si–Ge alloys. $In(CSe)_{1/2}$ has avery small direct band gap of 0.02 eV and could be used for far-infrared emitters and detectors also on Si–Ge alloys.

Finally, we investigated the bulk energetics and the initial growth energetics of $(ZnSi)_{1/2}P_{1/4}As_{3/4}$. The analyses show that $(ZnSi)_{1/2}P_{1/4}As_{3/4}$ and other Type I materials should indeed be possible to be grown using heteroepitaxial techniques.

ACKNOWLEDGMENTS

We would like to thank Professor S. Louie for his generosity in providing us with GW computer codes and E. Chang and B. Králik for their help with these codes. This work was supported in part by the Office of Naval Research Contract No. N0001-94-1-0591.

*Electronic address: tairan@mit.edu

[1] L. T. Canham, Appl. Phys. Lett. **57**, 1046 (1990).
[2] L. T. Canham, T. I. Cox, A. Loni, and A. J. Simons, Appl. Surf. Sci. **102**, 436 (1996).
[3] *Heteroepitaxy in Silicon II*, edited by J. Fan, J. Phillips, and B.-Y. Tsaur, MRS Symposia Proceedings No. 91 (Materials Research Society, Pittsburgh, 1987).
[4] R. F. Davis, Proc. IEEE **79**, 702 (1991).
[5] J. H. Edgar, J. Mater. Res. **7**, 235 (1992).
[6] J. C. R. Eddy, T. D. Moustakas, and J. Scanlon, J. Appl. Phys. **73**, 448 (1993).
[7] W. A. Harrison, E. A. Kraut, J. R. Waldrop, and R. W. Grant, Phys. Rev. B **18**, 4402 (1978).
[8] T. Wang, N. Moll, K. Cho, and J. D. Joannopoulos, Phys. Rev. Lett. **82**, 3304 (1999).
[9] L. J. Shay, *Ternary Chalcopyrite Semiconductors: Growth, Electronic Properties, and Applications* (Pergamon, Oxford, 1975).
[10] P. Hohenberg and W. Kohn, Phys. Rev. B **136**, 864 (1964).
[11] W. Kohn and L. J. Sham, Phys. Rev. A **140**, 1133 (1965).
[12] M. C. Payne, M. P. Teter, D. C. Allan, T. A. Arias, and J. D. Joannopoulos, Rev. Mod. Phys. **64**, 1045 (1992).
[13] I.-B. Sohrab and T. A. Arias, Comput. Phys. Commun. **128**, 1 (2000).
[14] J. P. Perdew and A. Zunger, Phys. Rev. B **23**, 5048 (1981).
[15] D. M. Ceperley and B. J. Alder, Phys. Rev. Lett. **45**, 566 (1980).
[16] A. M. Rappe, K. M. Rabe, E. Kaxiras, and J. D. Joannopoulos, Phys. Rev. B **41**, 1227 (1990).
[17] N. Troullier and J. L. Martins, Phys. Rev. B **43**, 1991 (1993).
[18] M. Fuchs and M. Scheffler (unpublished) http://www.fhiberlin.mpg.de/th/fhi96md/code.html.
[19] D. R. Hamann, Phys. Rev. B **40**, 2980 (1989).
[20] S. G. Louie, S. Froyen, and M. L. Cohen, Phys. Rev. B **26**, 1738 (1982).
[21] L. Kleinman and D. M. Bylander, Phys. Rev. Lett. **48**, 1425 (1982).
[22] J. Ihm, A. Zunger, and M. L. Cohen, J. Phys. C **12**, 4409 (1979).
[23] H. J. Monkhorst and J. D. Pack, Phys. Rev. B **13**, 5188 (1976).
[24] L. Hedin, Phys. Rev. A **139**, A796 (1965).
[25] L. Hedin and S. Lundqvist, in *Solid State Physics, Advances in Research and Application*, Vol. 23, edited by F. Seitz, D. Turnbull, and H. Ehrenreich (Academic, New York, 1969), p. 1.
[26] M. S. Hybertsen and S. G. Louie, Phys. Rev. B **34**, 5390 (1986).
[27] M. S. Hybertsen and S. G. Louie, Phys. Rev. B **37**, 2733 (1988).
[28] *Solar Energy Conversion*, Topics in Applied Physics, Vol. 31, edited by B. O. Seraphin (Springer-Verlag, Berlin, 1979).
[29] C. Kittel, *Introduction to Solid State Physics* (John Wiley & Sons, New York, 1996).
[30] R. M. Sieg, S. A. Ringel, S. M. Ting, S. B. Samavedam, M. Currie, T. Langdo, and E. A. Fitzgerald, J. Vac. Sci. Technol. B **16**, 1471 (1998).
[31] *Molecular Beam Epitaxy, Applications to Key Materials*, edited by R. F. C. Farrow (Noyes Publications, Park Ridge, New Jersey, 1995).
[32] J. L. House, D. J. Dougherty, G. S. Petrich, L. A. Kolodziejski, E. P. Ippen, and G.-C. Hua, Appl. Surf. Sci. **104-105**, 472 (1996).